

THE VELOCITY CENTROIDS GRADIENTS FOR ABSORBING MEDIA

DIEGO F. GONZÁLEZ-CASANOVA¹, A. LAZARIAN¹, AND BLAKESLEY BURKHART²*Draft version March 10, 2017*

ABSTRACT

We explore the application of the Velocity Gradient Technique, new way to trace magnetic fields in the plane of the sky, to an absorbing media for the case of ¹³CO 2-1 emission. Using MHD turbulence simulations, we calculate the velocity gradient using velocity centroids and an improved procedure for calculating gradients suggested by Yuen & Lazarian. We find that the velocity centroid gradients trace the projected magnetic field in media with different CO abundances, densities and optical depths. We also explore how the calculations of the magnetic field strengths, which employs the dispersion of the velocity gradient, is modified in the presence of self-absorption. Our study opens up the possibility to use velocity centroid gradients to trace magnetic fields using ¹³CO 2-1 emission.

Subject headings: ISM: magnetic fields, kinematics and dynamics - magnetohydrodynamics (MHD) - turbulence - molecular data - methods: observational

1. INTRODUCTION

Magnetic fields play fundamental role in astrophysical environments. They are important for the diffuse and for the dense molecular components of the interstellar medium (see [Draine 2011](#)). In particular, magnetohydrodynamic (MHD) processes are fundamental in Giant Molecular Clouds (GMCs) and the magnetic field can regulate star formation ([Crutcher 2012](#); [Burkhart et al. 2015](#); [Mocz et al. 2017](#)). GMCs' turbulence and magnetization is supported by measurements of line-width size relations, power spectra, and Zeeman measurements ([Ostriker 2003](#); [McKee & Ostriker 2007](#); [Crutcher 2012](#)). The Zeeman measurements also demonstrate that the support against self-gravity can come from magnetic pressure, and that the magnetic field energy can be comparable to turbulent kinetic energy ([Crutcher et al. 2010](#); [Draine 2011](#)). Because cloud conditions, such as the sonic and Alfvénic Mach numbers (M_S and M_A), affect the initial properties and outcomes of star-forming regions, is vital to better characterize the medium ([Burkhart et al. 2013a](#)). Furthermore, current understanding of protostar formation requires the presence of turbulence as a way to form the stars and remove/weaken the strong magnetic field presence in GMCs ([Hennebelle & Ciardi 2009](#); [Seifried et al. 2013](#); [González-Casanova et al. 2016](#)).

A new technique, namely, the Velocity Gradient Technique (VGT) was introduced by [González-Casanova & Lazarian \(2017, henceforth GL17\)](#) in order to study properties of interstellar magnetic field in observations. Using the modern theory of MHD turbulence (see [Brandenburg & Lazarian 2013](#), for a review and ref. therein) GL17 predicted that the velocity gradients should be perpendicular to the magnetic field and they used the observationally-available velocity centroids to prove this.

The VGT uses the principle that in MHD turbulence, the eddies align with the local magnetic field ([Goldreich & Sridhar 1995](#); [Lazarian & Vishniac 1999](#)). This

preferential direction generates a gradient in the velocity field that the VGT traces, and the velocity gradient is perpendicular to the magnetic field. In GL17 the velocity centroids gradients (VCGs) were studied for the synthetic observations without absorption, the setup that is relevant to the diffuse components of the interstellar medium (ISM), e.g. to diffuse atomic hydrogen. The results of the GL17 study demonstrated the ability of VCGs to trace magnetic fields and also be used to determine magnetic field strength using the approach similar to the famous Chandrasekhar-Fermi technique ([Chandrasekhar & Fermi 1953](#)).

The technique introduced in GL17 has recently been extended in ([Yuen & Lazarian 2017](#)), where a more accurate procedure for the calculation of the VCGs was suggested and the VCGs were applied to the GALFA HI data. The results were compared with the magnetic field directions as traced by *Planck* polarization maps and it was clearly demonstrated that in the diffuse media without self-gravity the tracing of magnetic fields is possible using the VCGs. This conclusion was in a good agreement with the results of the VCG analysis of the synthetic data in GL17. This same principle is also been proposed in Synchrotron polarized emission ([Burkhart et al. 2012](#); [Lazarian et al. 2017](#)).

The success of the VCGs as a new way to study ISM motivates us to revisit the problem and address the issue of whether the VCGs ability to trace magnetic field in diffuse media will be significantly affected by the effects of self-absorption. The effects of self-absorption can become important already for the HI and they are definitely important for ¹³CO 2 – 1, which we investigate in this paper. For our study we limit ourselves to the case when the gradients of velocities that arise from self-gravity are small compared to the gradients induced by MHD turbulence. We expect the former to be dominant near the centers of self-gravitating regions, e.g. in the vicinity of the forming stars, while for the vast expanses of the molecular gas we expect the MHD scaling to be applicable. This corresponds to the recent study in [Burkhart et al. \(2015\)](#) where the properties of the MHD turbulence were seen after the removal of the extreme concentrations of density. We further explore the applicability of the

casanova, lazarian @astro.wisc.edu

¹ Astronomy Department, University of Wisconsin-Madison, 475 North Charter Street, Madison, WI 53706-1582, USA² Harvard-Smithsonian Center for Astrophysics, 60 Garden St. Cambridge, MA 02138, USA

version of the Chandrasekhar-Fermi technique suggested in GL17 to the data with absorption.

The study of the VGT presented here, is done with different MHD conditions (compressibility and magnetization) and cloud properties (density and CO abundance). The dispersion of the velocity gradient can be then be used to determine the intensity of the magnetic field using an analog of the C-F method as used in GL17.

In what follows, in Section 2, we explore the theoretical approach of the VGT in PPV data; in Section 3, we describe the numerical code and setup of the simulations; in Section 4, we present the VGT in the presence of molecular emission; and in Section 6, we give our conclusions.

2. THEORETICAL CONSIDERATIONS

The theoretical motivation for the VGT is discussed in GL17. Here we briefly remind the reader why one may expect the alignment of VCGs perpendicular to the magnetic field. In strong MHD turbulence, the turbulence motions are eddy-like. In Alfvénic turbulence (Goldreich & Sridhar 1995) these eddies are aligned with their local magnetic field (Lazarian & Vishniac 1999; Cho & Vishniac 2000; Maron & Goldreich 2001), and the perpendicular l_\perp and parallel l_\parallel dimensions of the eddies are related by the “critical balance relation”:

$$l_\parallel^{-1} V_A \approx l_\perp^{-1} u_l, \quad (1)$$

where V_A is the Alfvén speed, and u_l is the eddy velocity. With the turbulence injection scale and velocity, respectively L , V_L , one can write for subAlfvénic turbulence, i.e. the turbulence with the Alfvén Mach number $M_A = V_L/V_A < 1$ (see Lazarian & Vishniac 1999):

$$\begin{aligned} l_\parallel &\approx L \left(\frac{l_\perp}{L} \right)^{2/3} M_A^{-4/3}, \\ u_l &\approx V_L \left(\frac{l_\perp}{L} \right)^{1/3} M_A^{1/3}, \end{aligned} \quad (2)$$

which shows that the disparity between l_\perp and l_\parallel is increasing with the decreasing the scale. Therefore one can expect the velocity gradients to be the largest perpendicular to the local direction of magnetic field. This way in MHD turbulence the velocity gradients can trace magnetic field.

In observations, the velocity gradients are obtained from the velocity centroid, S . S is the first order moment of the intensity and, as in the case of radio observations, the velocity centroid is measured by the antenna temperature:

$$S(\mathbf{X}) \propto \int v_z T(\mathbf{X}, v_z) dv_z, \quad (3)$$

where the integration is performed over the line-of-sight (LOS) component of velocity. By itself velocity centroids are a well-known measure and their use for tracing magnetic fields has also been previously demonstrated. For instance, in Esquivel & Lazarian (2005) and Burkhart et al. (2014) the anisotropies of the velocity centroid correlation functions were suggested to study the magnetic field direction.

3. DATA ANALYSED

We use the data-cubes from Burkhart et al. (2013a). These data cubes were obtained using the 3D numerical simulations generated by the compressible MHD code presented in (Cho & Lazarian 2002), which were post-processed to account for opacity effects using SimLine-3D software package Ossenkopf (2002). The details of the codes are described in the aforementioned papers as well as in the subsequent publications (see Burkhart et al. 2013b; Correia et al. 2014).

The synthetic observational data that we analyze assumes a box size of ~ 450 pc (corresponding to a cell size of ~ 5 pc), and a temperature of 10 K. The assumed telescope beam that produces the synthetic PPV intensity maps is $18''$ FWHM, with a velocity resolution of 0.05 Km s^{-1} . The number density, n , and the CO abundance, x_{co} , (the number-density ratio of CO/H₂), are changed by factors of 30 from the normal parameters (with 5 cases for each of the 10 MHD models—see Table 1). The normal parameters are set at a density of $n = 275 \text{ cm}^{-3}$ and abundance, $x_{co} = 1.5 \times 10^{-6}$, that represents typical values for GMCs. These changes allow investigation of line-saturation effects in the VGT.

We describe our simulation parameter set up in Table 1. Columns 2 and 3 give the magnetic field and pressure of the MHD simulations (B and p). Columns 5-9 denoted by Case gives the LOS averaged optical depth (τ_i). Column 5, τ_n , correspond to the normal case $n = 275 \text{ cm}^{-3}$ and CO abundance, $x_{co} = 1.5 \times 10^{-6}$. Column 6, τ_1 , correspond a lower density case $n_1 = n/30$. Column 7, τ_2 , correspond a higher density case $n_2 = 30 \cdot n$. Column 8, τ_3 , correspond to a lower CO abundance, $x_{co3} = x_{co}/30$. Column 9, τ_4 , correspond to a higher CO abundance, $x_{co4} = 30 \cdot x_{co}$. Both cases 1 and 2 have the same x_{co} as case normal and cases 3 and 4 have the same n as case normal.

4. ALIGNMENT OF VELOCITY GRADIENTS AND MAGNETIC FIELD

The VCGs calculations suggested in GL17 determines the direction of the maximum gradient of the velocity, defined in a circular center-punctured neighborhood around each point. In this work, however, we employ a different way of calculating velocity gradients that was suggested and tested in (Yuen & Lazarian 2017). The velocity centroid map is interpolated using the bicubic spline approximation over a rectangular mesh, adding 10 extra cells between each of the original points. At each of the original cells, \mathbf{X} , the VCG is defined as:

$$\Omega^S(\mathbf{X}) = \mathbf{X}', \quad (4)$$

where \mathbf{X}' is the direction where $\nabla^S(\mathbf{X})$ is maximum, \mathbf{X} and \mathbf{X}' are points in the plane of the sky. \mathbf{X}' is defined in an annulus with a radius of 10 cells around \mathbf{X} . $\nabla^S(\mathbf{X})$ is defined as:

$$\nabla^S(\mathbf{X}) = \max \left\{ \frac{|\mathbf{S}(\mathbf{X}) - \mathbf{S}(\mathbf{X} + \mathbf{X}')|}{|\mathbf{X}'|} \right\}. \quad (5)$$

This method of calculating VCGs provides better accuracy and a numerically more robust approach (Yuen & Lazarian 2017).

We compare the magnetic field direction inferred from the VCGs to the actual direction (obtained directly from

TABLE 1
DESCRIPTION OF THE SIMULATION USED

Model	B	p	M_S	Case normal	Case 1	Case 2	Case 3	Case 4
				τ_n $n = 275$ & $x_{co} = 1.5 \times 10^{-6}$	τ_1 $n = 9$	τ_2 $n = 8250$	τ_3 $x_{co} = 5 \times 10^{-8}$	τ_4 $x_{co} = 4.5 \times 10^{-5}$
A	1	1	0.7	3.22	0.323	49.8	0.232	52.2
B	1	0.7	1	3.48	0.355	54.7	0.252	57.2
C	1	0.1	2	3.52	0.348	54.1	0.235	57.2
D	1	0.05	4	3.21	0.344	54.5	0.207	57.4
E	1	0.01	7	3.45	0.376	62.0	0.213	65.0

Note: Column 1 indicates the letter for the model for the MHD simulation given by the parameters in Columns 2-4. In Columns 5-9, we show the map-averaged optical depths for the different cases of our radiative transfer parameter space applied to the MHD simulations. This produces a total of 5 MHD models with 5 cases each. For our radiative transfer parameter space, we vary both the number density scaling factor (in units of cm^{-3} , denoted with the symbol n) and the molecular abundance ($^{13}\text{CO}/\text{H}_2$, denoted with the symbol x_{co}) in order to change excitation and optical depth τ . To represent the typical parameters of a molecular cloud, we choose standard values for density, $n = 275 \text{ cm}^{-3}$, and abundance, $x_{co} = 1.5 \times 10^{-6}$ (what we will refer to as the normal parameter setup shown in Column 5). The cloud parameters density and abundance are changed by factor of 30 larger and smaller giving the values of Columns 6-9. Thus, Column 6, denoted by τ_1 , has parameters: $n = 8250 \text{ cm}^{-3}$, and abundance, $x_{co} = 1.5 \times 10^{-6}$. Column 7, denoted by τ_2 , has parameters: $n = 9 \text{ cm}^{-3}$, and abundance, $x_{co} = 1.5 \times 10^{-6}$. Column 8, denoted by τ_3 , has parameters: $n = 275 \text{ cm}^{-3}$, and abundance, $x_{co} = 4.5 \times 10^{-5}$. Column 9, denoted by τ_4 , has parameters: $n = 275 \text{ cm}^{-3}$, and abundance, $x_{co} = 5 \times 10^{-8}$.

the simulations) of the magnetic field by projecting it to the plane of the sky:

$$\begin{aligned} \mathbf{B}_x(\mathbf{X}) &\propto \int \mathbf{B}_x(\mathbf{X}, z) dz, \\ \mathbf{B}_y(\mathbf{X}) &\propto \int \mathbf{B}_y(\mathbf{X}, z) dz, \end{aligned} \quad (6)$$

where, \mathbf{X} , denotes the plane of the sky vector, z is measured along the LOS, and the mean magnetic field is perpendicular to the LOS. The alignment between two vectors, i.e. the local projected magnetic field and the VCGs can be quantized by the angle between them, ϕ . Figure 1 shows the histograms of the angle distribution between VCG and \mathbf{B} given by the 5 different MHD initial conditions and the 5 cloud conditions. Each panel corresponds to a MHD model and the different colors corresponds to the different n and x_{co} values. The histograms (the measurements of the angle distribution) are made after a Gaussian smoothing kernel with a standard deviation of two is apply to the VCG data. It is clear that the sonic Mach number affects the gradient, but in most cases the gradient is present independent of the CO density/abundance in the cloud (n and x_{co}). This suggests that CO can be used in regard to the VCG method.

To further quantify the alignment we measure the spread in the distribution, σ_ϕ , using the standard deviation of the angle distribution, ϕ . Figure 2 in the bottom panel shows σ_ϕ as a function of average optical depth. The values for the optical depth are shown in Table 1 and correspond to the different cloud environments. A different way to visualize σ_ϕ is as a function of the sonic Mach number for the different cases (see Figure 3). The lack of a clear trend in Figure 3 is likely due to numerical artifacts on the simulations, rather than underlying physical properties because of the small deviations.

The measurement of σ_ϕ requires the knowledge of the magnetic field, but independently one can always measure the spread a distribution of the VCGs directions. The corresponding measure σ is the standard deviation of VCG distribution and is independent of \mathbf{B} . Since σ is an independent measurement it can be used to measure the strength of the magnetic field as we describe in

subsection 4.1. σ and σ_ϕ are different quantities that measures the width of the distribution and are different from the Gaussian smoothing kernel apply to the data.

Figure 2 shows the dependence of σ and σ_ϕ on the optical depth τ and is clear that a higher optical depth has better the alignment. The better alignment arises because the higher τ is, the smaller the LOS average of the turbulent eddies becomes. In other words, a high τ reduces the amount of eddies along the LOS, the less eddies produces a clearer measurement of the MHD velocity gradient.

4.1. Analog of Chandrasekhar-Fermi technique for the VGT

The Chandrasekhar & Fermi (1953, C-F) method is a technique to determine the intensity of the magnetic field in the ISM using two approximations: MHD motions are assumed to be Alfvénic, and the dispersion of the magnetic field is traced by the dispersion in the polarization measurements. Subsequent studies have analyzed the method to better constrain the polarization dispersion and the coefficient (Ostriker et al. 2001; Falceta-Gonçalves et al. 2008; Houde et al. 2009; Novak et al. 2009):

$$B_{CF} = \gamma \sqrt{4\pi\rho} \frac{\sigma^S}{\sigma_\phi}, \quad (7)$$

where γ is the empirical coefficient, σ^S is the dispersion in the velocity measured by the velocity centroid, σ_ϕ is the dispersion of the dust polarization, ρ is the ambient density, and B_{CF} is the estimated magnetic field intensity.

GL17 expanded the C-F method, incorporating the dispersion in the velocity gradient instead of the dispersion of the dust alignment. The physics of the approach remains, but now the dispersion of the magnetic field is measured by the VCG rather than by dust polarization. In the classical C-F method, $\gamma \sim 0.5$, while for the modified method $\gamma \sim 1.29$ (with no self-absorption). We now expand it to self-absorption media, in particular CO emission with $\gamma \sim 0.02$. The value of γ is the averaged on all the values estimated individually for each model and case. The small value is due to the higher densities relative to the ones found in H I (see Table 1).

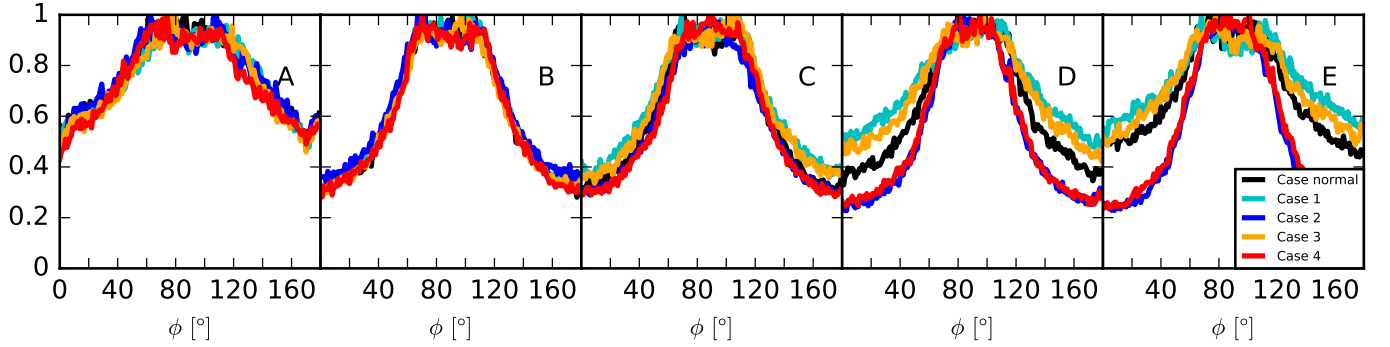


FIG. 1.— Histogram of the angle distribution of the intensity gradient for all models. Each panel corresponds to one model and has the corresponding letter (see Table 1). M_S increases from left to right. The different colors correspond to the different cases (variations in density and x_{co}). *Black* is the normal conditions, *cyan* is the low density case (case 1), *blue* is the high density case (case 2), *orange* is the low x_{co} (case 3), and *red* is the high x_{co} (case 4). The histograms are set to have 1 as the maximum value to compare with different resolutions. The VCG maps are smooth using a Gaussian kernel with a standard deviation of 2.

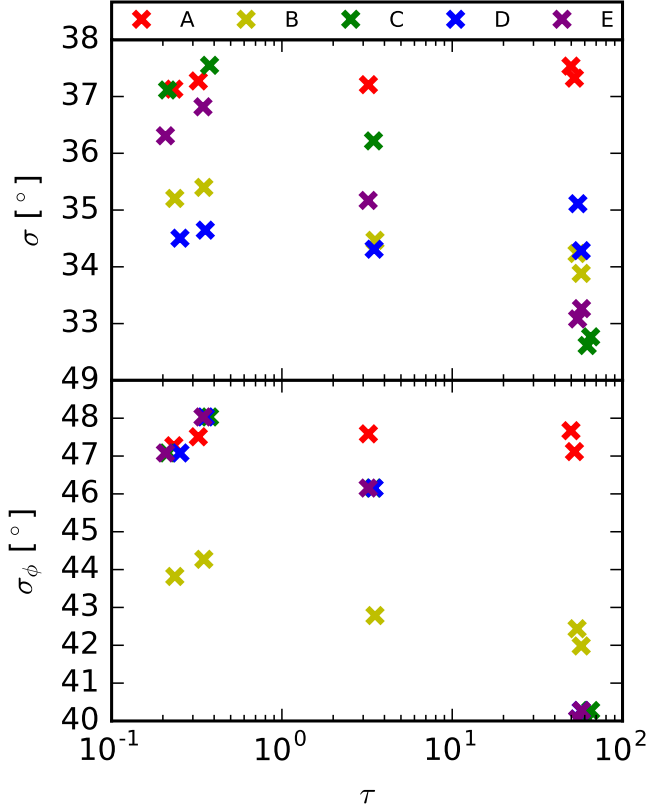


FIG. 2.— *Top Panel:* σ as a function of the optical depth, τ . *Bottom Panel:* σ_ϕ as a function of τ . The different colors correspond to the different models, labeled by their letter (see Table 1).

The velocity dispersion σ^S is obtained from the MHD simulation and therefore is the same for all the cases per model. The values for the density are found in Table 1, and the angle dispersion in Figure 3. Figure 4 shows the errors of our C-F method using the VCG. To account for the variability in densities used in our calculations (9 to 8250 cm^{-3}), we normalized the errors by the squared root of the density.

4.2. Gaussian Fit

The angle distribution for all cases and models shows a peak at 90° , implying that most cells have a good correspondence between the VCG and **B**. The spread in the distribution, however, implies a natural dispersion, due to statistical process and the nature of MHD media (Esquivel & Lazarian 2010). In order to reduce the impact of the distribution's natural dispersion and understand better the local-global properties, we divided the data into sub-blocks.

At each sub-block we found the peak of the distribution for both the VCG and the magnetic field. It is then imposed that the direction of each sub-block is given by the most common direction, i.e. the peak. The direction obtained, represents a local-global property (and therefore, the direction fluctuates between sub-blocks). The intensity map (in log space) and the local-global directions are found in Figure 5. This process to obtain the local-global direction of the magnetic fields makes the VGT a statistical technique, in the sense that it does not give the actual direction of the magnetic field at each cell, but still gives a local picture. With this process

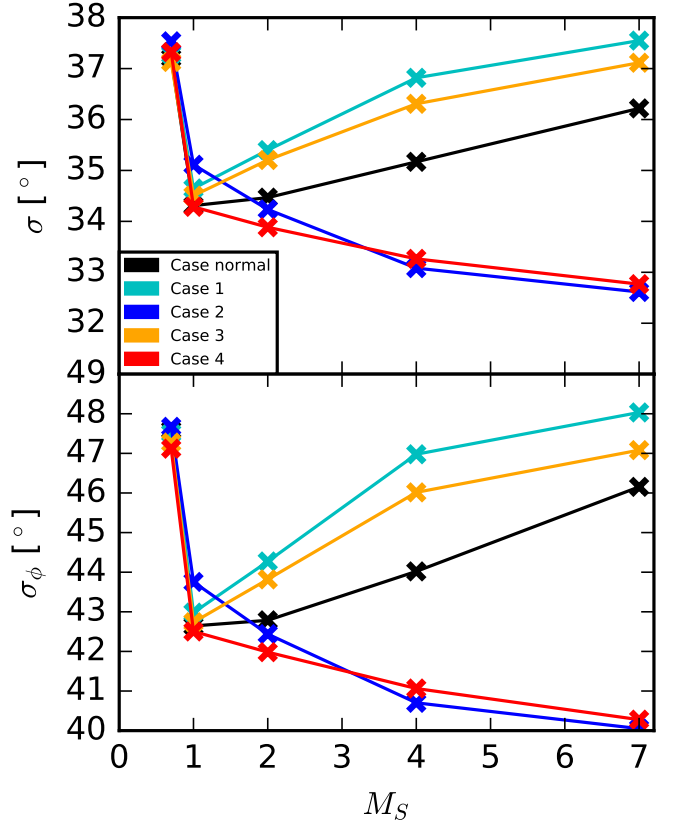


FIG. 3.— *Top Panel:* σ as a function of M_S . *Circles.* *Bottom Panel:* σ_ϕ as a function of M_S . The different colors correspond to the different cases (variations in density and x_{co}). *Black* is the normal conditions, *cyan* is the low density case (case 1), *blue* is the high density case (case 2), *orange* is the low x_{co} (case 3), and *red* is the high x_{co} (case 4).

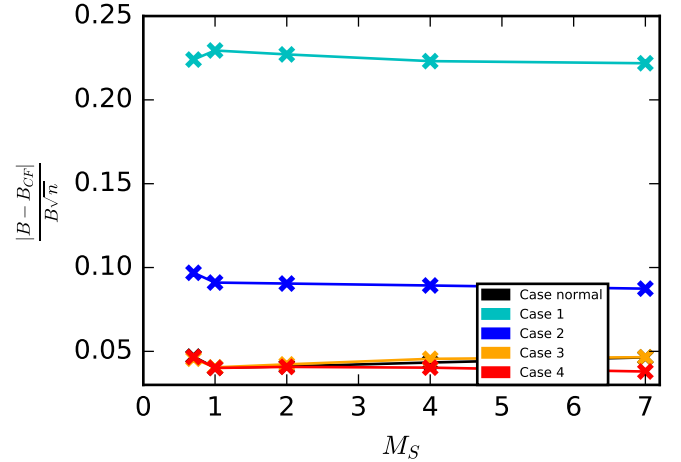


FIG. 4.— Uncertainties in the estimates of the magnetic field strength using the modified C-F method as a function of M_S . The density normalization comes to account for the different densities (see Table 1). The different colors correspond to the different cases (variations in density and x_{co}). *Black* is the normal conditions, *cyan* is the low density case (case 1), *blue* is the high density case (case 2), *orange* is the low x_{co} (case 3), and *red* is the high x_{co} (case 4).

the alignment between the VCG and the magnetic field increases, as seen in Figure 5.

The size of each sub-block is dependent on the local alignment. As seen in Yuen & Lazarian (2017) depending

on the conditions of the sub-block, more or less cells are needed to get a Gaussian like distribution to determine the maximum. It is then important consider the compressibility and magnetization, that produces the alignment, when deterring the size of the sub-block. Figure 5 presents this analysis with a sub-block size of 100^2 cells.

The larger the sub-block the more points and there fore the better the constrains on the distribution. To asses the effects of the sub-block size in the calculations we estimated the reduction factor, R . The reduction factor is analogous to the Rayleigh factor used in dust alignment theory and has been used in the context of the VGT (Greenberg 1968).

$$R = 2 \left\langle \cos(\phi)^2 - \frac{1}{2} \right\rangle, \quad (8)$$

where ϕ is the angle between the VCG and the magnetic field. R ranges from -1 to 1, with $R = 1$ for a parallel configuration and $R = -1$ for a perpendicular one. The reduction factor is measured for different block sizes for each of the models and cases. Figure 6 shows R for 2 models and each of their 5 cases. It is clear that for the sub-Alfvénic regimen the R decreases implying a better perpendicular alimnet as the sub-block size increases. And for all the sub-block sizes a good alignment ($R \ll 0$). Overall the larger the sub-block, the better the alignment, but even at small sizes there is a good correspondence.

5. COMPARISON WITH OTHER TECHNIQUES

Estimating the strength and direction of the magnetic field in GMCs is important to understand both star formation and GMC dynamics. The direction of the magnetic field can be obtain by polarization measurements. The alignment of dust grains with the magnetic field that produces the polarization depends on the dust properties, making it dependent on the dust model. Furthermore, at high optical depths, there is no non-degenerate method for resolving the direction of the magnetic field, limiting the applicability of dust alignment theory (Lazarian & Hoang 2007; Lazarian et al. 2015).

Statistical techniques can aid in measuring the anisotropy of the velocity fluctuations, which is necessary to determine the strength and direction of the magnetic field. These techniques include anisotropies in PPV (Lazarian et al. 2002; Esquivel et al. 2015), correlations of velocity centroids (Esquivel & Lazarian 2005), Principal Component Analysis (PCA) (Heyer et al. 2008), higher-order statistical moments (Kowal et al. 2007; Burkhart et al. 2009), velocity centroid anisotropies (Kandel et al. 2016), and the “ Δ -variance” technique (a wavelet transformation) (Stutzki et al. 1998; Mac Low & Ossenkopf 2000). These techniques, statistical in nature, can only give global properties of the medium.

The importance of the VGT is that it can measure the local direction of the magnetic field and that is independent of dust polarization nor on more global measurements. The VGT can produce both the strength and direction of the magnetic field only using spectroscopic data. As seen the VGT produces better results at high optical depths, making it a great tool to understand GMC.

6. CONCLUSIONS

This works expands the Velocity Gradient Technique (VGT) to ^{13}CO 2-1 emission, exploring a new method for measuring magnetic field in molecular media. The VGT presents a way of tracing magnetic fields using only the velocity centroid, which can be obtained from spectroscopic data. The method is based on the fact that the eddies align with the local 3D magnetic field, which creates eddies whose velocity gradients are perpendicular to the direction of the field. A summary of the work is as follows:

1. The VGT is able to trace magnetic fields in sub-Alfvénic, and sub- & supersonic regimes for molecular emission with self absorption. The alignment works similarly for all densities and CO abundances.
2. We extended the use of the Chandrasekhar-Fermi to estimate the level of magnetization in molecular media, only requiring spectroscopic observations and the density of the medium.
3. We employ the fact that the VGT produces a distribution that is Gaussian-like, and use the peak of this distribution to determine a local-global direction of the magnetic field. With this approach we are able to increase the accuracy of the technique, having a better measurement of the direction of the magnetic field.

We are grateful to Ka Ho Yuen for the fruitful discussion of the results and procedures of gradient calculation. We thank Zach Pace for the insightful discussions. AL and DFGC are supported by the NSF grant AST 1212096. Partial support for DFGC was provided by CONACyT (Mexico). AL acknowledges a distinguished visitor PVE/CAPES appointment at the Physics Graduate Program of the Federal University of Rio Grande do Norte and thanks the INCT INEspaço and Physics Graduate Program/UFRN, at Natal, for hospitality. BB is supported by the NASA Einstein Postdoctoral Fellowship.

REFERENCES

- Brandenburg, A. and Lazarian, A. 2013, Space Sci. Rev., 178, 163
 Burkhart, B., Collins, D. C., and Lazarian, A. 2015, ApJ, 808, 48
 Burkhart, B., Falceta-Gonçalves, D., Kowal, G., and Lazarian, A. 2009, ApJ, 693, 250
 Burkhart, B., Lazarian, A., and Gaensler, B. M. 2012, ApJ, 749, 145
 Burkhart, B. et al. 2014, ApJ, 790, 130
 Burkhart, B., Lazarian, A., Ossenkopf, V., and Stutzki, J. 2013a, ApJ, 771, 123
 Burkhart, B., Ossenkopf, V., Lazarian, A., and Stutzki, J. 2013b, ApJ, 771, 122
 Chandrasekhar, S. and Fermi, E. 1953, ApJ, 118, 113
 Cho, J. and Lazarian, A. 2002, Physical Review Letters, 88, 245001
 Cho, J. and Vishniac, E. T. 2000, ApJ, 539, 273

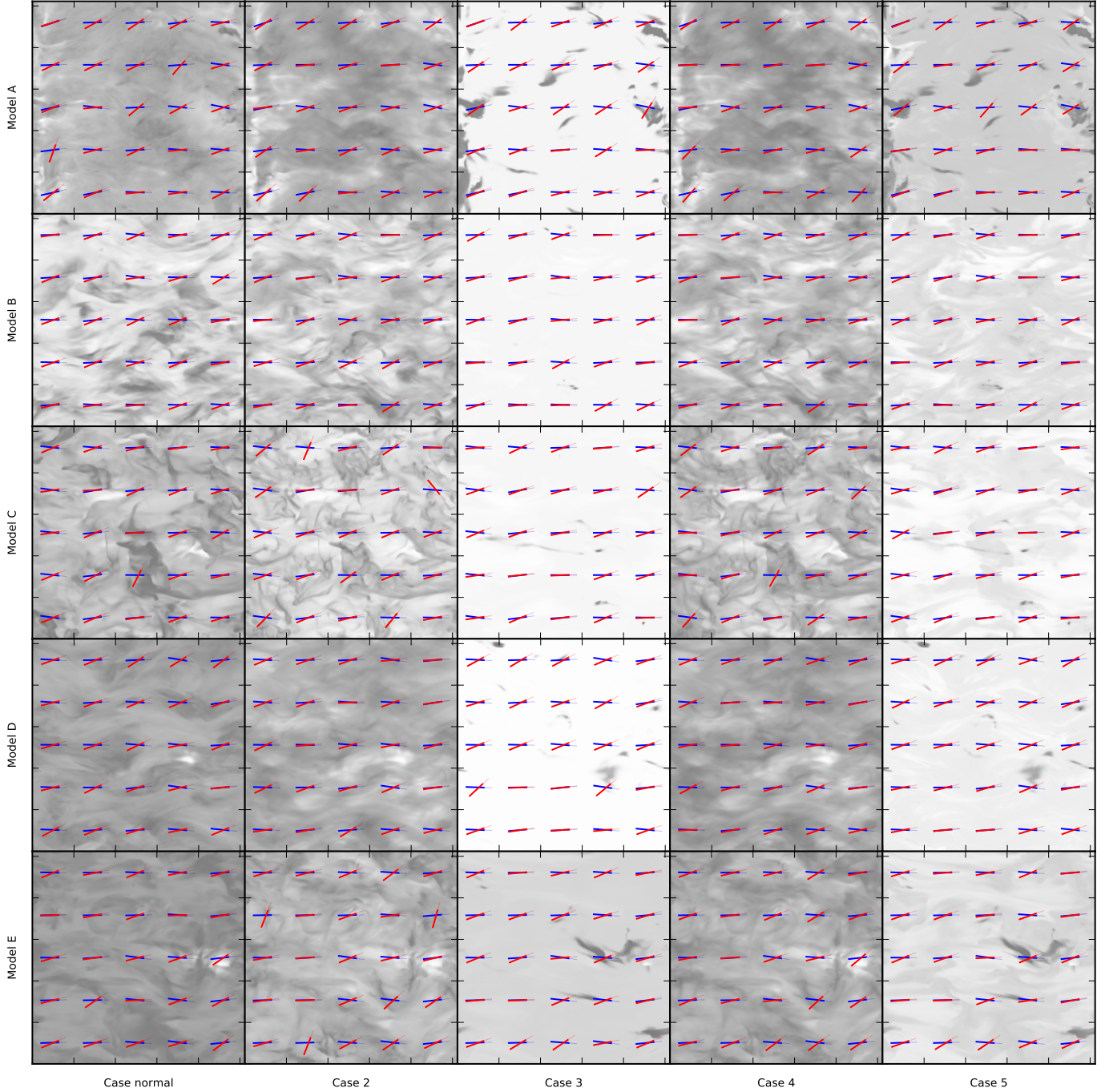


FIG. 5.— The intensity map (log scaled), with the vector field of the VCG, Ω , rotated 90° and plotted over in *red*; and the direction of the magnetic field (in the plane of the sky) plotted over in *blue*. Both directions are given by the peak of the distribution after a Gaussian kernel is used. Each row corresponds to a different model, and each column to a case. The sub-block size is 100^2 cells.

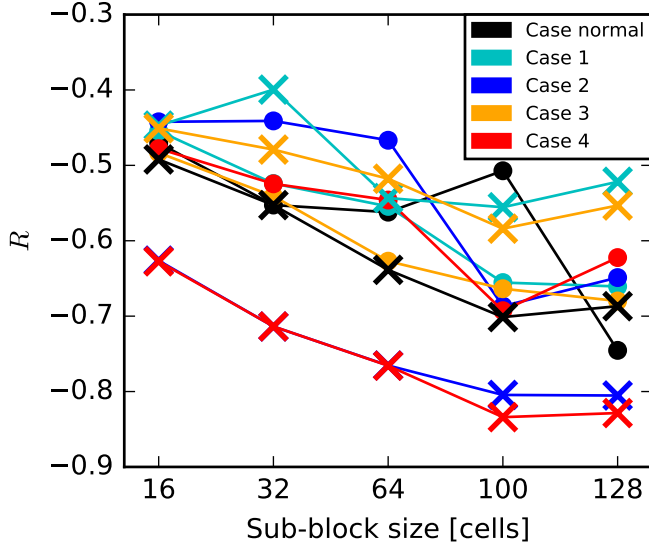


FIG. 6.— The reduction factor, as a function of the sub-block size for models A (*crosses*) & E (*dots*). The different colors correspond to the different cases (variations in density and x_{co}). *Black* is the normal conditions, *cyan* is the low density case (case 1), *blue* is the high density case (case 2), *orange* is the low x_{co} (case 3), and *red* is the high x_{co} (case 4).

Correia, C. et al. 2014, ApJ, 785, L1
 Crutcher, R. M. 2012, ARA&A, 50, 29
 Crutcher, R. M. et al. 2010, ApJ, 725, 466
 Draine, B. T. 2011, Physics of the Interstellar and Intergalactic Medium (Princeton University Press)
 Esquivel, A. and Lazarian, A. 2005, ApJ, 631, 320
 —. 2010, ApJ, 710, 125
 Esquivel, A., Lazarian, A., and Pogosyan, D. 2015, ApJ, 814, 77
 Falceta-Gonçalves, D., Lazarian, A., and Kowal, G. 2008, ApJ, 679, 537

Goldreich, P. and Sridhar, S. 1995, ApJ, 438, 763
 González-Casanova, D. F. and Lazarian, A. 2017, ApJ, 835, 41
 González-Casanova, D. F., Lazarian, A., and Santos-Lima, R. 2016, ApJ, 819, 96
 Greenberg, J. M. 1968, Nebulae and interstellar matter, ed. B. M. Middlehurst & L. H. Aller, Vol. VII (the University of Chicago Press)
 Hennebelle, P. and Ciardi, A. 2009, A&A, 506, L29
 Heyer, M., Gong, H., Ostriker, E., and Brunt, C. 2008, ApJ, 680, 420
 Houde, M. et al. 2009, ApJ, 706, 1504
 Kandel, D., Lazarian, A., and Pogosyan, D. 2016, MNRAS
 Kowal, G., Lazarian, A., and Beresnyak, A. 2007, ApJ, 658, 423
 Lazarian, A., Andersson, B.-G., and Hoang, T. 2015, Grain alignment: Role of radiative torques and paramagnetic relaxation, 81
 Lazarian, A. and Hoang, T. 2007, MNRAS, 378, 910
 Lazarian, A., Pogosyan, D., and Esquivel, A. 2002, in Astronomical Society of the Pacific Conference Series, Vol. 276, Seeing Through the Dust: The Detection of HI and the Exploration of the ISM in Galaxies, ed. A. R. Taylor, T. L. Landecker, & A. G. Willis, 182
 Lazarian, A. and Vishniac, E. T. 1999, ApJ, 517, 700
 Lazarian, A., Yuen, K. H., Lee, H., and Cho, J. 2017, ArXiv e-prints
 Mac Low, M.-M. and Ossenkopf, V. 2000, A&A, 353, 339
 Maron, J. and Goldreich, P. 2001, ApJ, 554, 1175
 McKee, C. F. and Ostriker, E. C. 2007, ARA&A, 45, 565
 Mocz, P. et al. 2017, ArXiv e-prints
 Novak, G., Dotson, J. L., and Li, H. 2009, ApJ, 695, 1362
 Ossenkopf, V. 2002, A&A, 391, 295
 Ostriker, E. C. 2003, in Lecture Notes in Physics, Berlin Springer Verlag, Vol. 614, Turbulence and Magnetic Fields in Astrophysics, ed. E. Falgarone & T. Passot, 252–270
 Ostriker, E. C., Stone, J. M., and Gammie, C. F. 2001, ApJ, 546, 980
 Seifried, D., Banerjee, R., Pudritz, R. E., and Klessen, R. S. 2013, MNRAS, 432, 3320
 Stutzki, J. et al. 1998, A&A, 336, 697
 Yuen, K. H. and Lazarian, A. 2017, ArXiv e-prints